
The Computer Synthesis of Expressive Faces

Keith Waters and Demetri Terzopoulos

Phil. Trans. R. Soc. Lond. B 1992 **335**, 87-93
doi: 10.1098/rstb.1992.0011

Email alerting service

Receive free email alerts when new articles cite this article - sign up in the box at the top right-hand corner of the article or click [here](#)

The computer synthesis of expressive faces

KEITH WATERS¹ AND DEMETRI TERZOPOULOS²

¹Digital Equipment Corporation, Cambridge Research Lab, One Kendall Square, Cambridge, Massachusetts 02139, U.S.A.

²Department of Computer Science, University of Toronto, Toronto, Ontario M5S 1A4, Canada

SUMMARY

This paper presents a methodology for the computer synthesis of realistic faces capable of expressive articulations. A sophisticated three-dimensional model of the human face is developed that incorporates a physical model of facial tissue with an anatomical model of facial muscles. The tissue and muscle models are generic, in that their structures are independent of specific facial geometries. To synthesize specific faces, these models are automatically mapped onto geometrically accurate polygonal facial representations constructed by photogrammetry of stereo facial images or by non-uniform meshing of detailed facial topographies acquired by using range sensors. The methodology offers superior realism by utilizing physical modelling to emulate complex tissue deformations in response to coordinated facial muscle activity. To provide realistic muscle actions to the face model, a performance driven animation technique is developed which estimates the dynamic contractions of a performer's facial muscles from video imagery.

1. INTRODUCTION

One of the hardest challenges in the field of computer graphics animation has been to develop computational models of the face capable of synthesizing various nuances of facial motion quickly and convincingly. The difficulty of the task is primarily due to the intricate physical structure of the face: the skeletal foundation has an elaborate, highly curved surface, to which are attached specialized muscles mediating facial expression. The muscles are embedded into deformable skin tissue, which has a layered composition and complex viscoelastic properties. Previous graphics models have ignored the underlying structure of the face, crudely approximating it as a simple surface subject to *ad hoc* geometric deformations.

This paper undertakes a more thorough emulation of the face to enhance the quality of facial animation. A hierarchical model is described that incorporates knowledge about the psychology of human facial expression, the anatomy of facial muscle structures, the histology of facial tissues, and the physics of deformable materials (Terzopoulos & Waters 1990). In particular, two deformable tissue models are developed that approximate facial tissue elasto-dynamics: a tri-layered model that reflects the layered structure of skin and a simplified, bi-layered model which is easier to construct and computationally less expensive. The synthetic tissues deform in response to a parametric muscle model that takes the actions of the primary facial muscles into consideration. Despite its sophistication, the face model can be computed and rendered at rapid screen refresh rates on a high performance graphics workstation.

The tissue and muscle models are generic, in that

their structures are independent of specific facial geometries. To create instances of synthetic faces, such as those illustrated in this paper, the tissue and muscle models must be mapped onto geometric representations of individual faces. Suitable polygonal representations may be acquired through manual measurement by using a three-dimensional digitizer, through photogrammetry of stereo facial images, or through meshing of optical range sensor data. The proposed facial modelling techniques may be applied generically to all these data sources and across the wide range of facial geometries evident in humans. This stands in contrast to prior models that offered a limited range of performable actions restricted to specific facial geometries.

The face model described in this paper provides a natural set of control parameters that are based on the muscular motivators of real faces. The required time-varying control inputs correspond to the contractions of the major muscles underlying human facial expression. Inputs suitable for realistically animating the face may be generated manually, or they may be derived from video sequences of human performers. Estimating dynamic muscle contractions from facial-image sequences poses an interesting image analysis problem. A solution is described that applies deformable contour models to track features undergoing non-rigid motions in the image plane (Terzopoulos & Waters 1990).

2. BACKGROUND

This section presents a brief historical perspective of facial modelling and animation in computer graphics.

The first attempts in facial animation involved key-framing, where two or more complete facial expressions are captured and inbetween frames computed by interpolation (Parke 1972). The immense variety of facial expressions makes this approach extremely data intensive, and this prompted the development of parametric models for facial animation.

Parametric facial models (Parke 1974, 1982) create expressions by specifying sets of parameter value sequences; for instance, by interpolating the parameters rather than direct keyframing. The parameters control facial features, such as the mouth opening height, width, and protrusion. However, if parameters are not specified with care the model will produce incorrect shapes, unrealistic motions, and other spurious effects. The limitations of *ad hoc* parameterized models prompted a movement towards models whose parameters are based on the anatomy of the face (Platt 1980; Platt & Badler 1981; Waters 1987; Waite 1989; Magnenat-Thalmann *et al.* 1988). Such models operate with parameters based on facial muscle structures. When anatomically based models incorporate facial action coding schemes (Ekman 1977) as control procedures, it becomes relatively straightforward to synthesize a range of recognizable expressions.

The limited realism achievable with geometric facial models is primarily due to their failure to account for the fact that the face is an elaborate biomechanical system. In particular, it appears difficult to mimic in a purely geometric way many of the subtle physically based deformations of skin, such as bulging and wrinkling (Komatsu 1988). Studies of tissue mechanics (Kenedi *et al.* 1975) have led to finite element approximations with application to surgical simulation (Larrabee 1986; Deng 1988), but such models are computationally expensive. For graphics applications a simple, efficient deformable lattice serves well as a tissue model (Pieper 1989; Waters & Terzopoulos 1990).

Performance-driven animation is emerging as an important issue for animating faces with a high degree of visual fidelity (Williams 1990; Terzopoulos & Waters 1990). In contrast to the significant effort

devoted to parametric facial modelling, the inverse problem of extracting parameters from images of real faces has received little attention. Some relevant work has focussed on the subproblem of lip synchronization, but the parameter extraction techniques remain predominantly manual (Brook & Summerfield 1983; Lewis & Parke 1987; Thalmann *et al.* 1988; Hill *et al.* 1988). It is fairly easy to establish a correspondence between video footage of a performer and an animate face model using intrusive schemes – for instance, by tracking markers placed on the performer's face to coincide with deformation control points on the model (Williams 1990) – but it is worthwhile to search for less intrusive methods of estimating control parameters from video sequences of faces in motion.

3. FACIAL TISSUE MODELING

(a) *Skin histology and mechanics*

Human skin has a layered structure. The epidermis, a superficial layer of dead cells, is about one tenth the thickness of the dermis that it protects. The layered structure of skin is non-homogeneous and non-isotropic (Kenedi *et al.* 1975; Larrabee 1986) (e.g. lower stiffness along Langer's lines than across them).

The mechanical properties of skin are due mostly to the dermal tissue. Dermal tissue is composed of collagen (72%) and elastin (4%) fibres forming a densely convoluted network in a gelatinous ground substance (20%). Under low stress, dermal tissue offers low resistance to stretch as the collagen fibres begin to uncoil, but under greater stress the uncoiled collagen fibres resist stretch much more markedly. This yields a biphasic stress–strain curve (figure 1). The incompressible ground substance retards the motion of the fibres and thereby gives rise to time-dependent viscoelastic behaviour: stress relaxation at constant strain, strain creep at constant stress, and hysteresis under cyclic loading. Finally, the elastin fibres act like elastic springs which return the collagen fibres to their uncoiled condition under zero load.

(b) *Deformable lattices*

Facial tissue may be approximated as a discrete deformable model (Terzopoulos & Fleischer 1988), a lattice of point masses connected by springs. Let node i , where $i = 1, \dots, N$, be a point mass m_i with position $\mathbf{x}_i(t) = [x(t), y(t), z(t)]'$, velocity $\mathbf{v}_i = d\mathbf{x}_i/dt$, and acceleration $\mathbf{a}_i = d^2\mathbf{x}_i/dt^2$. Let spring k have natural length L_k and stiffness c_k . Suppose it connects node i to node j , where $\mathbf{r}_k = \mathbf{x}_j - \mathbf{x}_i$ is the vector separation of the nodes. The actual length of the spring is $l_k = \|\mathbf{r}_k\|$. The deformation of the spring is $e_k = l_k - L_k$ and the force the spring exerts on node i is defined as

$$\mathbf{s}_k = (c_k e_k / l_k) \mathbf{r}_k. \quad (1)$$

A biphasic spring is defined by the stiffness

$$c_k = \begin{cases} \alpha_k & \text{when } e_k \leq e_k^c; \\ \beta_k & \text{when } e_k > e_k^c; \end{cases}$$

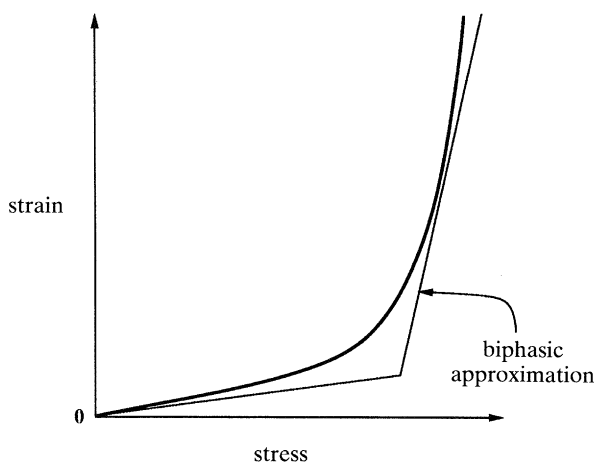


Figure 1. Stress-strain curve of facial tissue and its biphasic approximation.

where α_k is smaller than β_k . Like dermal tissue, the biphasic spring is readily extensible at small strains, but exerts increased restoring stresses past a critical strain ϵ^c .

The discrete Lagrange equation of motion for the node/spring lattice is the system of coupled, second order ordinary differential equations

$$m_i \frac{d^2 \mathbf{x}_i}{dt^2} + \gamma_i \frac{d\mathbf{x}_i}{dt} + \sum_{j \in \mathcal{N}_i} \mathbf{s}_{kj} + \mathbf{q}_i = \mathbf{f}_i; \quad i = 1, \dots, N. \quad (2)$$

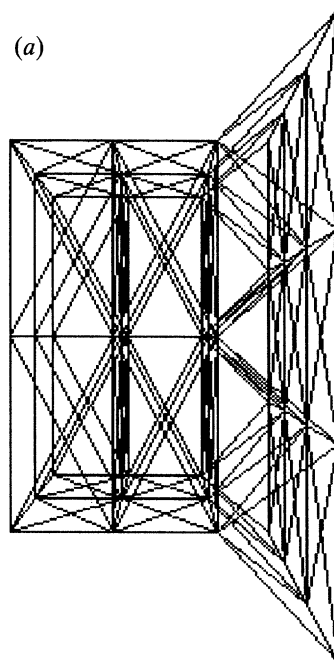
Here, γ_i is a coefficient of velocity-dependent damping that models kinetic energy dissipation through friction in the facial tissue to provide an artificial viscoelastic response. The summation indicates the force on node i due to springs which connect it to other nodes $j \in \mathcal{N}_i$. To account for the incompressibility of the cutaneous ground substance and the subcutaneous fatty tissues, a constraint is included into the lattice which approximately conserves its volume as it deforms; this constraint yields volume preservation forces \mathbf{q}_i acting on each node in the lattice. Finally, the forces \mathbf{f}_i account for external influences on the tissue, such as the collisions between lips and teeth.

To simulate the dynamics of the lattice, initial positions \mathbf{x}_i^0 and velocities $\mathbf{v}_i^0 = \mathbf{0}$ are provided for each node $i = 1, \dots, N$, and the equations of motion are numerically integrated forward through time using an efficient, explicit Euler procedure (Terzopoulos & Waters 1990). The stability of the Euler procedure is limited (Press *et al.* 1986), but its convergence is facilitated by the damping in the lattice and the flexibility of the biphasic springs in the small-strain region.

(c) Layered tissue models

A portion of a tri-layered facial tissue model is shown in figure 2. Each line in the figure represents a biphasic spring. The springs are arranged into layers of pentahedral elements and hexahedral elements cross-strutted with springs to resist shearing and twisting stresses. The springs in the three layers – representing cutaneous tissue, subcutaneous tissue, and the muscle layer – have different stiffness parameters in accordance with the non-homogeneity of real facial tissue. The topmost surface of the lattice represents the epidermis (a rather stiff layer of keratin and collagen) and the spring stiffnesses are set to make it moderately resistant to deformation. The springs underneath the epidermis form pentahedral elements which represent the dermis. The springs in the second layer, which contains hexahedral elements, are highly deformable, reflecting the nature of subcutaneous fatty tissue. Nodes at the bottom of the second layer represent the fascia to which the muscle fibres that run through the hexahedral elements in the third layer are attached. Nodes on the bottommost surface of the lattice are fixed in ‘bone’.

The tri-layered tissue model is nontrivial to construct and computationally expensive to simulate. Trading accuracy for efficiency, the first two layers may be approximated by a single layer of hexahedral elements, yielding a simplified bi-layered tissue model.



(b)

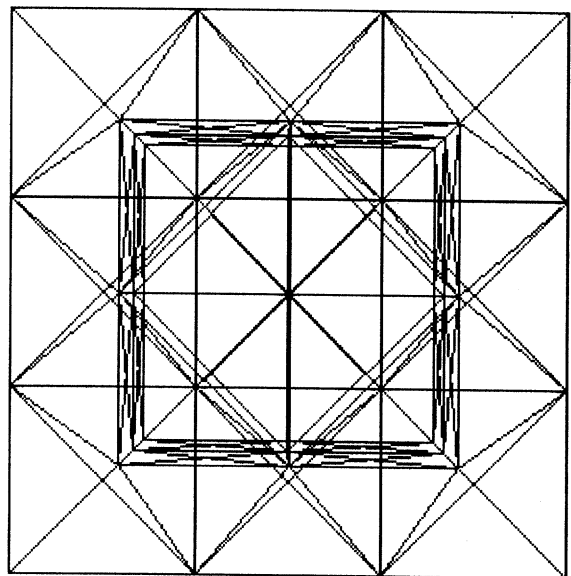


Figure 2. A tri-layered facial tissue model (a) top view; (b) side view.

The uniform structure of the bi-layered model makes it easy to map onto facial geometries constructed from range sensor data (see § 5).

4. FACIAL MUSCLE MODELLING

In human faces, over 200 voluntary muscles can exert traction on the facial tissue to create expressions. When individual muscles contract, they displace the facial tissue to which they attach towards the place where they emerge from the underlying skeletal framework.

(a) Parametric muscle model

Although it is difficult to simulate the actions of all the muscles in the human face a broad range of facial expression may be synthesized using a small set of primary muscle actuators (Waters 1987).

Let \mathbf{m}_i^e denote the point where muscle i emerges from the bone, and \mathbf{m}_i^a its point of attachment in the tissue. These two points specify a muscle vector

$$\mathbf{m}_i = \mathbf{m}_i^e - \mathbf{m}_i^a.$$

The displacement of node j from \mathbf{x}_j to \mathbf{x}_j' due to muscle contraction is a weighted sum of m muscle activities on node j :

$$\mathbf{x}_j' = \mathbf{x}_j + \sum_{i=1}^m c_i b_{ij} \mathbf{m}_i, \quad (3)$$

where $0 \leq c_i \leq 1$ is a muscle contraction factor and b_{ij} is a muscle blend function. Defining $\mathbf{r}_{ij} = \mathbf{m}_i^a - \mathbf{x}_j$,

$$b_{ij} = \begin{cases} \cos\left(\frac{\|\mathbf{r}_{ij}\|\pi}{a_i}\right) & \text{for } \|\mathbf{r}_{ij}\| \leq a_i; \\ 0 & \text{otherwise,} \end{cases} \quad (4)$$

where a_i is the radius of influence of the cosine blend profile.

Once all the muscle interactions have been computed, the lattice nodes \mathbf{x}_j are displaced to their new positions \mathbf{x}_j' . As a result, those nodes not influenced by the muscle contraction are in an unstable state and forces propagate through the lattice to establish a new equilibrium.

(b) Coordinating muscle activities

Ekman and Friesen have proposed the Facial Action Coding System (FACS), a quantified abstraction of the action of facial muscles, as a means of recording facial expressions independent of cultural or personal interpretation (Ekman 1977). The FACS represents facial expressions in terms of 66 action units (AUs) grouped into the upper face and the lower face, and they include vertical actions, horizontal actions, oblique actions, orbital actions, and miscellaneous

actions. The face model incorporates a simplified FACS interpreter implemented as part of an earlier parameterized muscle model consisting of approximately 20 muscle actuators (Waters 1987). The interpreter is capable of producing a broad range of facial expressions by translating action units into coordinated muscle activities.

5. ASSEMBLING FACIAL MODELS

To create synthetic faces, the tissue and muscle models must be assembled and conformed to realistic facial geometries. The facial geometries illustrated in this paper are derived from two sources: photogrammetry of stereo images (Parke 1972) and meshing of range data acquired with optical scanners (Cyberware 1990). Both acquisition techniques yield polygonal facial geometries.

Starting with a non-uniform triangular facial mesh derived through photogrammetry, a layered tissue model may be assembled. To assemble a tri-layered model, the nodes and springs of the initial mesh represent the epidermis. Normal vectors from the centre of gravity of each triangle are projected below the surface of the face to establish nodes at the subcutaneous tissue interface. Tetrahedral units are then constructed by attaching springs from the epidermis triangle nodes to the new nodes. The new springs represent the dermal layer. Short weak springs are then attached from the second layer to another set of nodes to form the subcutaneous layer. A final set of springs is attached from these nodes and anchored to the bone, thus establishing the muscle layer. The muscle fibres are then inserted through the muscle layer from their emergence in bone to their nodes of attachment. The complete facial model in figure 3 was constructed in this way. The bi-layered tissue model may be constructed in analogous fashion.

High speed active range sensing is a source of accurate geometric and photometric facial data. Typically, 128×10^3 range and reflectance samples can be captured in a few seconds providing a very detailed map of a person's head (figure 4) (Cyberware 1990). From a practical standpoint, this much data is exces-

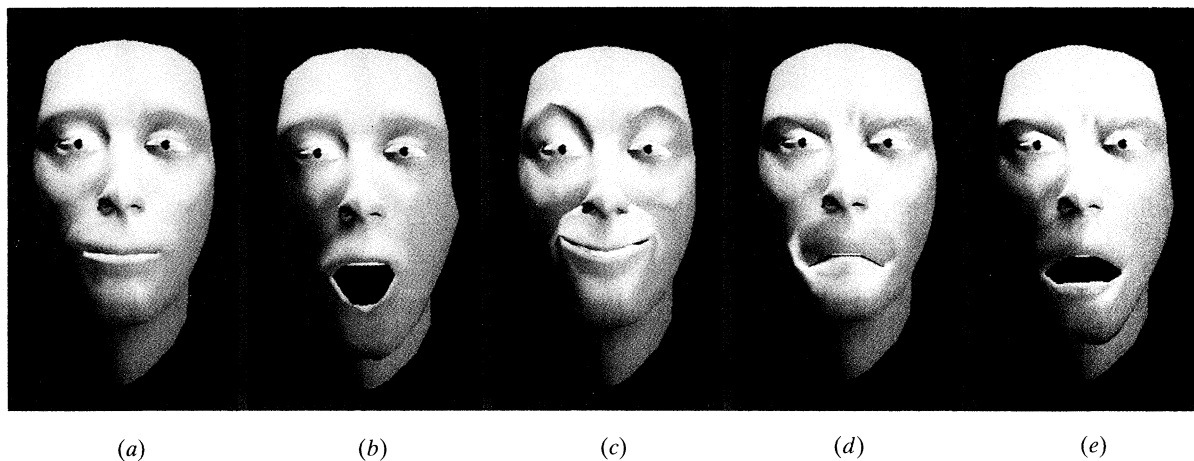


Figure 3.

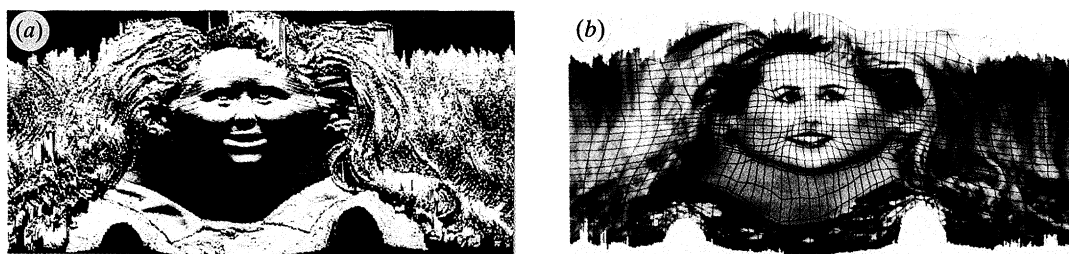


Figure 4.

sive, especially in flat regions of the face, and should be reduced to a manageably sized polygonal mesh.

An adaptive meshing technique (Terzopoulos & Vasilescu 1991) can be used to design coarser, non-uniform meshes capturing the essential structure of the high resolution facial maps. These meshes automatically adapt to features of interest in the data, increasing polygon density over articulate facial areas, for instance. The high-resolution colour photometric map may easily be texture mapped onto the polygonal surface, restoring the illusion of detail (Oka *et al.* 1987; Yau & Duffy 1988; Williams 1990). Figure 5a illustrates a three-dimensional texture-mapped facial model. The model was constructed by using an adaptive mesh (dark lines in figure 4b) to sample the radial range map in figure 4a, thus generating an accurate three-dimensional facial mesh. The adaptive mesh also provided texture coordinates that were employed to paint the colour photometric map shown in figure 4b onto the facial mesh.

(a) Facial animation examples

The above facial models are efficient enough to simulate and render at screen refresh rates greater than 8 Hz on a single Central Processing Unit (CPU) of a Silicon Graphics Iris 4D-240VGX workstation. The bi-layered and tri-layered models were used to generate figures 3a–3e, figures 5a–c, and figure 6c. See Terzopoulos & Waters (1990) for details regarding the numerical simulation parameters.

Figures 3a–3e and figure 6c use a tri-layered model of facial tissue. Figure 3a shows the undeformed facial tissue model. Figure 3b shows the jaw rotated. Figure 3c illustrates the concentration of the zygomatic major

muscles and the frontalis major muscles. Figure 3d shows the contraction of the lateral corrugator and the anguli depressors, and figure 3e shows the same muscle contractions with the jaw open. Note the wrinkles in the skin that appear around the frowning mouth of the model. This effect, although difficult to accomplish with a purely geometric model, emerges automatically through the physical simulation of the facial tissue, principally due to the volume preservation constraints.

Figures 5a–c use a bi-layered model. Figure 5a is the static facial geometry, figure 5b shows a non-symmetric contraction of the zygomatic major and the frontalis outer. Figure 5c is a symmetrical contraction of the anguli depressors and a raising of the frontalis inner.

6. ANALYSIS OF DYNAMIC FACIAL IMAGES

This section describes a method for measuring some of the dynamic characteristics of the facial expressions of a human performer which may subsequently be used to animate a facial model. This is accomplished by estimating dynamic contractions of the performer's facial muscles from video sequences of his or her face. The method makes use of deformable contours (Kass *et al.* 1987) to track the non-rigid motions of salient facial features, such as the mouth and eyebrows, over successive video frames.

(a) Deformable contours

A discrete deformable contour (Terzopoulos & Waters 1990) is defined as a set of nodes indexed by $i=1, \dots, n$ that are connected in series by springs.

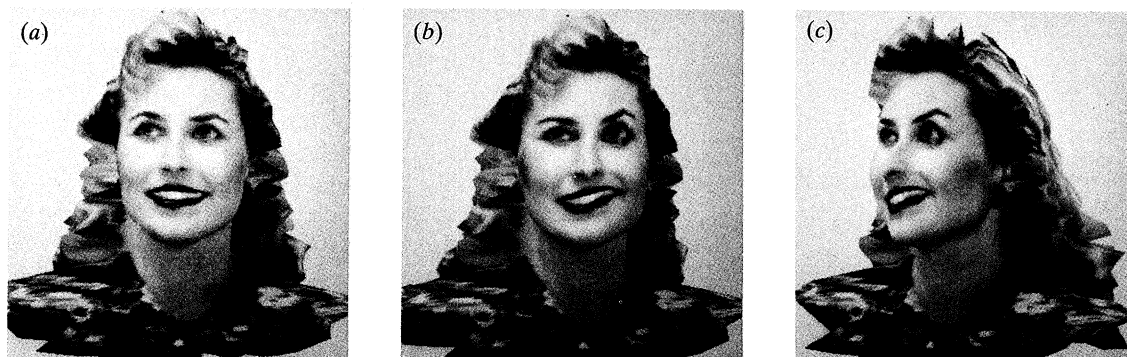


Figure 5.

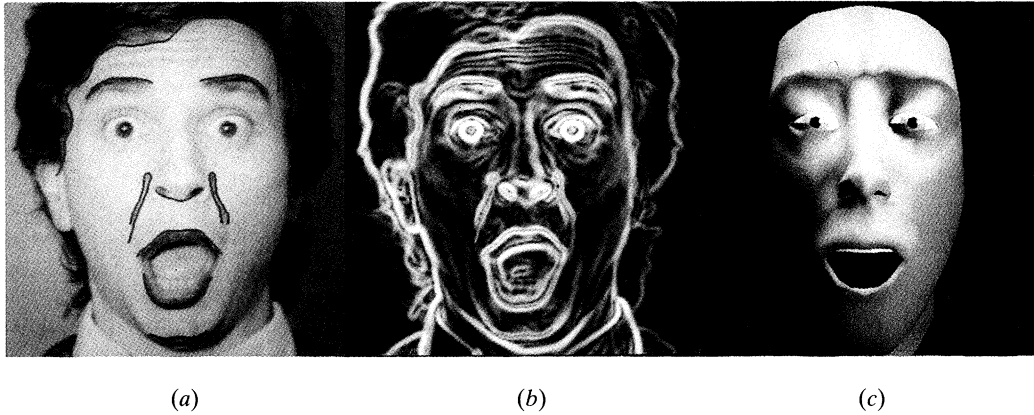


Figure 6.

Associated with these nodes are time varying positions $\mathbf{x}_i(t) = [x_i(t), y_i(t)]'$ in the image plane. An interactive deformable contour results from numerically simulating the first-order dynamical system

$$\gamma \frac{d\mathbf{x}_i}{dt} + \boldsymbol{\alpha}_i + \boldsymbol{\beta}_i = \mathbf{f}_i; \quad i = 1, \dots, n, \quad (5)$$

where γ is a velocity-dependent damping constant, $\boldsymbol{\alpha}_i(t)$ and $\boldsymbol{\beta}_i(t)$ are 'tension' and 'rigidity' forces internal to the contour, and $\mathbf{f}_i(t)$ are external forces acting in the image plane.

Following the formulation of equation (1), let l_i be the natural length of the spring connecting node i to node $i+1$, and let $\mathbf{r}_i = \mathbf{x}_{i+1} - \mathbf{x}_i$ be the separation of the nodes and $e_i = \|\mathbf{r}_i\| - l_i$ be the deformation. Hence,

$$\boldsymbol{\alpha}_i = \frac{a_i e_i}{\|\mathbf{r}_i\|} \mathbf{r}_i, \quad (6)$$

where a_i is a tension variable. A viscoelastic contour may be obtained by letting $dl_i/dt = v_i e_i$, where v_i is a coefficient of viscoelasticity. Next,

$$\boldsymbol{\beta}_i = b_{i+1}(\mathbf{x}_{i+2} - 2\mathbf{x}_{i+1} + \mathbf{x}_i) - 2b_i(\mathbf{x}_{i+1} - 2\mathbf{x}_i + \mathbf{x}_{i-1}) + b_{i-1}(\mathbf{x}_i - 2\mathbf{x}_{i-1} + \mathbf{x}_{i-2}), \quad (7)$$

where b_i are rigidity variables. Tension, rigidity, and viscoelasticity are locally adjustable though the a_i , b_i , and v_i variables.

The deformable contour is responsive to a force field, derived from the image, which influences its shape and motion. It is convenient to express the force field through a time-varying potential function $P(x, y, t)$. A user may also interact with the deformable contour by applying forces $\mathbf{f}_i^z(t)$ using a mouse (Kass *et al.* 1987). Combining the two types of forces results in

$$\mathbf{f}_i = p \nabla P(\mathbf{x}_i) + \mathbf{f}_i^z, \quad (8)$$

where p is the strength of the image forces and

$$\nabla = [\partial/\partial x, \partial/\partial y]'$$

is the gradient operator in the image plane.

(b) Image processing and facial feature tracking

To apply deformable contours to facial image analysis, the image intensity function $I(x, y, t)$ at time t

is transformed into a planar force field using image processing techniques. The procedure is illustrated in figure 6. From the facial image in figure 6a, a two-dimensional potential function $P(x, y, t)$ is created whose ravines (extended local minima) coincide with the significant intensity changes associated with facial features such as the eyebrows, mouth, and chin. This is accomplished by computing the magnitude of the gradient of the image intensity

$$P(x, y, t) = -\|\nabla G_\sigma * I(x, y, t)\|, \quad (9)$$

where G_σ denotes convolution with a Gaussian smoothing filter of width σ that broadens the ravines so that they attract the contours from a distance. Figure 6b shows the negative of $P(x, y)$ computed from the frame in figure 6a.

The contours 'slide downhill' in $P(x, y, t)$ (for fixed t) and come to equilibrium at the bottoms of the nearest ravines, thus conforming to the shapes of the facial features of interest. Once the contours have settled into ravines of the current image, the next image is introduced and the contours again slide into the displayed ravines, so long as the movement of facial features is small. This procedure is repeated on subsequent frames to track the non-rigid motions of the facial features. As the deformable contours evolve, their dynamic state variables \mathbf{x}_i^z provide quantitative information about the non-rigid shapes and motions of the facial features.

(c) A facial image analysis example

Several facial expressions of a performer were videotaped in frontal view and a surprise sequence was analysed. Figure 6 illustrates the analysis of one of the frames in the sequence, showing nine deformable contours (black curves in figure 6a, white in figure 6b) in their final equilibrium positions locked onto the left and right eyebrows, the left and right nasolabial furrows, the tip of the nose, the upper and lower lips, and the chin boss. From the state variables of the deformable contours, the following are automatically estimated:

head reference point from the average position of the hairline contour; contractions of the left and right zygomaticus major from the positions of the endpoints of the upper lip contour; contraction of the left and right levator labii superioris alaeque nasi from the positions of the uppermost points of the associated nasolabial furrow contours; contractions of the left and right inner, major, and outer occipitofrontalis, respectively, from the positions of the innermost, centre, and outermost points of the associated eyebrow contours; jaw rotation from the average position of the chin boss contour.

The estimated muscle contractions may be converted to dynamic contraction factors (c_i in equation (3)) and input to the face model to reconstruct the expression. A frame of the reconstructed surprise is shown in figure 6c.

7. CONCLUSION

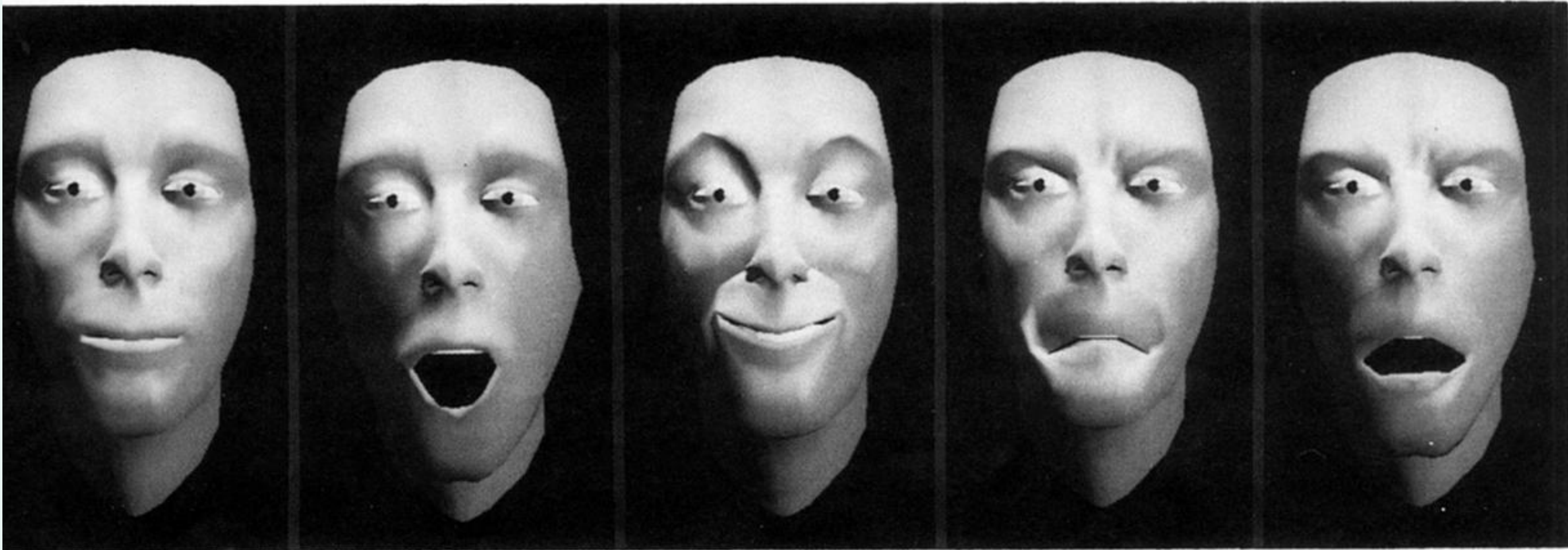
A methodology for the realistic modelling and animation of computer generated faces was presented. A synthetic tissue model was described which emulates the biomechanics of real skin. Techniques were proposed for mapping the synthetic tissue onto acquired facial geometries and for incorporating a parametric facial muscle model. A semi-automatic approach for extracting muscle control parameters from video images of real faces was described.

The research reported herein was done by the authors at the Schlumberger Laboratory for Computer Science, Austin, Texas. D. Terzopoulos is a Fellow of the Canadian Institute for Advanced Research.

REFERENCES

- Brooke, N.M. & Summerfield, S. 1983 Analysis, synthesis, and perception of visible articulatory movements. *J. Phonet.* **11**, 63–76.
- Cyberware Laboratory, Inc. 1990 *4020/RGB 3D scanner with color digitizer*. Monterey, California.
- Deng, X. 1988 A finite element analysis of surgery of the human facial tissues. Ph.D. thesis, Columbia University.
- Ekman, P. & Friesen, W.V. 1977 *Manual for the facial action coding system*. Palo Alto: Consulting Psychologists Press.
- Hill, D., Pearce, A. & Wyvill, B. 1988 Animating speech: An automated approach using speech synthesised by rules. *Vis. Comput.* **3**, 277–287.
- Kass, M., Witkin, A. & Terzopoulos, D. 1987 Snakes: active contour models. *J. Comput. Vis.* **1**(4), 321–331.
- Kenedi, R.M., Gibson, T., Evans, J.H. & Barbenel, J.C. 1975 Tissue mechanics. *Physics Med. Biol.* **20**(5), 699–717.

- Komatsu, K. 1988 Human skin model capable of natural shape variation. *Vis. Comput.* **3**, 265–271.
- Larrabee, W. 1986 A finite element model of skin deformation. I Biomechanics of skin and soft tissue: a review. *Laryngoscope* **96**, 399–405. II An experimental model of skin deformation. *Laryngoscope* **96**, 406–412. III The finite element model. *Laryngoscope* **96**, 413–419.
- Lewis, J.P. & Parke, F.I. 1987 Automated lipsynch and speech synthesis for character animation. *Proceedings of Human Factors in Computing Systems, Toronto*, 143–147.
- Oka, M., Tsutsui, K., Ohba, A., Kurauchi, Y. & Tago, T. 1987 Real-time manipulation of texture mapped surfaces. *Comput. Graph.* **21**(4), 181–188.
- Parke, F.I. 1972 Computer generated animation of faces. M.Sc. thesis, Technical Report UTEC-CSc-72-120, Department of Computer Science, University of Utah.
- Parke, F.I. 1974 A parametric model for human faces. Ph.D. thesis, Technical Report UTEC-CSc-75-047, Department of Computer Science, University of Utah.
- Parke, F.I. 1982 Parameterized models for facial animation. *IEEE Comput. Graph. Applic.* **2**(9), 61–68.
- Pieper, S. 1989 More than skin deep: physical modeling of facial tissue. M.Sc. thesis, Massachusetts Institute of Technology.
- Platt, S.M. 1980 A system for computer simulation of the human face. M.Sc. thesis, University of Pennsylvania.
- Platt, S.M. & Badler, N.I. 1981 Animating facial expressions. *Comput. Graph.* **15**(3), 245–252.
- Press, W., Flannery, B., Teukolsky, S. & Vetterling, W. 1986 *Numerical recipes: the art of scientific computing*. Cambridge University Press.
- Terzopoulos, D. & Vasilescu, M. 1991 Sampling and reconstruction with adaptive meshes. *Proceedings of Computer Vision and Pattern Recognition Conference (CVPR-91), Lahaina, Hawaii*, 70–75.
- Terzopoulos, D. & Fleischer, K. 1988 Deformable models. *Vis. Comput.* **4**(6), 306–331.
- Terzopoulos, D. & Waters, K. 1990 Physically-based facial modeling, analysis, and animation. *J. Visual. Anim.* **1**(2), 73–80.
- Magenat-Thalmann, N., Primeau, E. & Thalmann, D. 1988 Abstract muscle action procedures for face animation. *Vis. Comput.* **3**, 290–297.
- Waite, C. 1989 The facial action control editor, FACE: a parametric facial expression editor for computer generated animation. M.Sc. thesis, Massachusetts Institute of Technology.
- Waters, K. 1987 A muscle model for animating three-dimensional facial expression. *Comput. Graph.* **22**(4), 17–24.
- Waters, K. & Terzopoulos, D. 1990 A physical model of facial tissue and muscle articulation. *Proceedings of the First Conference on Visualization in Biomedical Computing (VBC'90), Atlanta, Georgia*, 77–82.
- Williams, L. 1990 Performance-driven facial animation. *Comput. Graph.* **24**(4), 235–242.
- Yau, J.F.S. & Duffey, N.D. 1988 A texture mapping approach to 3-D facial image synthesis. *Comput. Graph. Forum*, **7**, 129–134.



(a)

(b)

(c)

(d)

(e)

Figure 3.

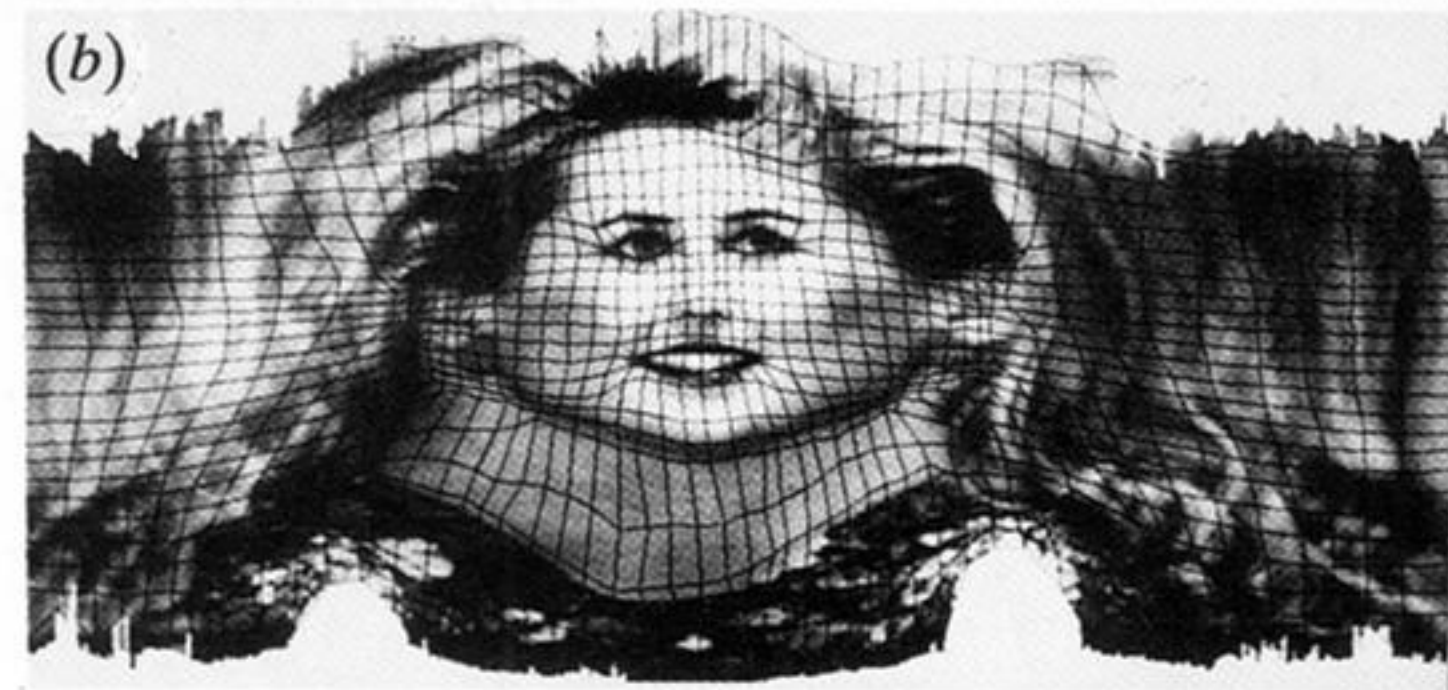


Figure 4.

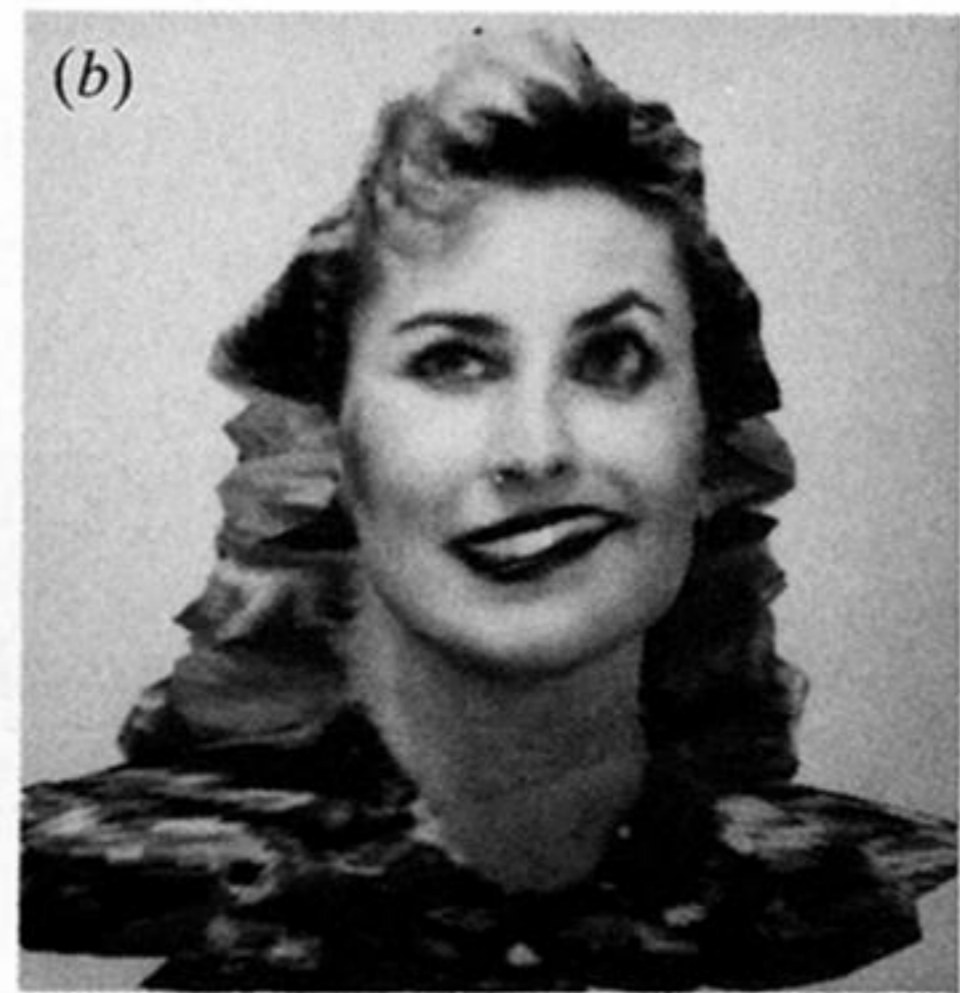


Figure 5.



(a)



(b)



(c)

Figure 6.